Water Supply

IWA PUBLISHING

Water Supply Vol 22 No 4, 4015 doi: 10.2166/ws.2022.031

3D numerical simulation of dam-break flow over different obstacles in a dry bed

Reza Maghsoodi[a], Abdolghafour Khademalrasoul[b] and Hamed Sarkardeh[c,*]

[a] Department of Civil Engineering, Faculty of Engineering, Esfarayen University of Technology, Esfarayen, Iran
[b] Faculty of Civil Engineering and Architecture, Shahid Chamran University of Ahvaz, Ahvaz, Iran
[c] Department of Civil Engineering, Faculty of Engineering, Hakim Sabzevari University, Sabzevar, Iran
*Corresponding author. E-mail: sarkardeh@hsu.ac.ir

ABSTRACT

In this research, a numerical investigation was carried out on the effect of obstacle presence on the water flow during the dam-break in a dry bed. The validity of the numerical simulations was confirmed after comparing the results with the experimental evidence. Rectangular, trapezoidal and triangle obstacles were simulated numerically to explain the obstacle effect on the water flow. Water surface tracking and turbulent flow were modeled using the Volume of Fluid (VOF) method and the standard k-ω model, respectively. Pressure and velocity variations during the dam-break flow are presented and analyzed.

Key words: dam-break, Fluent software, free surface flow, standard k-ω model, VOF

HIGHLIGHTS

- Simulation of dam-break flow.
- Presence of an obstacle in the flow.
- Different obstacle geometries.
- Numerical verification of water surface.
- Pressure distributions during flow after dam-break.

1. INTRODUCTION

Dams are one of the most important artificial structures to protect human lives and preserve water supplies. Therefore, the constructors commonly attempt to ensure the safety of the dams during the operation period. The designers are faced with the dam-break because it is a possible accidental problem. From this point of view, numerous experimental, numerical modeling and analytical studies have been conducted on dam failure (Lobovský *et al.* 2014). Ritter (1892) used an analytical solution with the Saint-Venant equations to the dam-break flow, in which the resistance was neglected. Dressler (1952) considered the Chezy resistance formula added to the nonlinear shallow water equations for the dam-break solution when resistance is neglected. Lauber & Hager (1998) studied dam-break waves in a smooth rectangular and horizontal channel. Goater & Hogg (2011) used the nonlinear shallow water equations for a collapse of a reservoir into an initially stationary layer of fluid. Maghsoodi *et al.* (2012) investigated dam-break with a stationary object using Computational Fluid Dynamics (CFD). Wang & Pan (2015) used shallow water equations to model the dam-break down a uniform slope. Akkerman *et al.* (2011) investigated dam-break with a stationary object using isogeometric analysis. Amini *et al.* (2016) used isogeometric analysis so that the governing Navier-Stokes (NS) equations using a pressure projection method are solved in a Lagrangian form. Shobeyri & Afshar (2010) offered a discrete least squares meshless method for the simulation of incompressible free surface flows in a Lagrangian form using a pressure projection method. Yu *et al.* (2016) proposed a Coupled Level Set (CLS)/Immersed Boundary (IB) method developed in Cartesian grids. In recent years, numerous experimental tests have been carried out on dam-break. Morris (2000) employed a triangular bump for numerical verification of dam-break flow propagation. Ozmen-Cagatay & Kocaman (2011) presented an experimental and numerical investigation of dam-break flow over initially dry bed with a trapezoidal obstacle. They used Flow-3D for solving the Reynolds Averaged Navier Stokes (RANS) equations with the k-ω turbulence model and the Shallow Water Equations (SWE). Soares-Frazão & Zech (2007) presented data about the effect of such an obstacle on a dam-break wave. The experimental setup consisted in a channel with a rectangular shaped

obstacle, which was a representation of a building. Issakhov *et al.* (2018) presented the effect of water on obstacles in the dam-break flow problem.

Yang *et al.* (2018) utilized FLOW-3D software to investigate the distribution and differences of turbulence kinetic energy and also presented a comprehensive understanding of dam-break wave generation and propagation. Gu *et al.* (2018) used a 3D interface-preserving level set method to simulate dam-break flow problems. In this paper dam-break problems either with or without obstacles were studied to confirm the coupled two-phase incompressible flow and level set method solver. Seyedashraf *et al.* (2017) proposed a novel technique based on Artificial Neural Network (ANN) along with an equation and detailed solution of the 1D dam-break problems without source terms. Celis *et al.* (2017) investigated dam breaking and sloshing forces based on Finite Difference Method (FDM). Heo *et al.* (2017) developed a CLS-VOF (volume of fluid) and IB method, and applied it to simulating the interaction between dam-break flow and stationary obstacles. Munoz & Constantinescu (2020) investigated a 3D, non-hydrostatic, RANS model using the VOF approach to simulate dam-break flows. Vosoughi *et al.* (2020) evaluated multiphase flood waves caused by failure of silted-up dams experimentally and numerically. Ye *et al.* (2020) employed a mesh-free method to simulate dam-break wave spreading in different bed configurations.

Although several studies have been made on the analysis of the dam-break, there is a lack of information on the effect of different obstacle geometries on flood flow. For this purpose, in the current study the dam-break flow was investigated by solving the NS and multiphase flow equations for an incompressible fluid. Also, various forms of obstacles were considered in a dry bed. Finally, results were compared with other researches.

2. MATERIALS AND METHODS

2.1. Experimental data collected

In this contribution, three experimental dam-break cases were considered in order to numerically investigate the turbulent water flow surfaces over the obstacles after dam-break. The first case was an experimental model (Akkerman *et al.* 2011) with a rectangular tank consisting of a 1.22 m × 1 m × 0.55 m column of water with the object located at 2.315 m from the beginning of the channel with dimensions 0.161 m × 0.161 m × 0.403 m (Figure 1).

In the second case, the model (Ozmen-Cagatay & Kocaman 2011) consisted of a rectangular tank as a horizontal channel 8.9 m long and 0.30 m wide. The column of water was 4.65 m × 0.3 m × 0.25 m. In this model a symmetrical trapezoidal-shaped

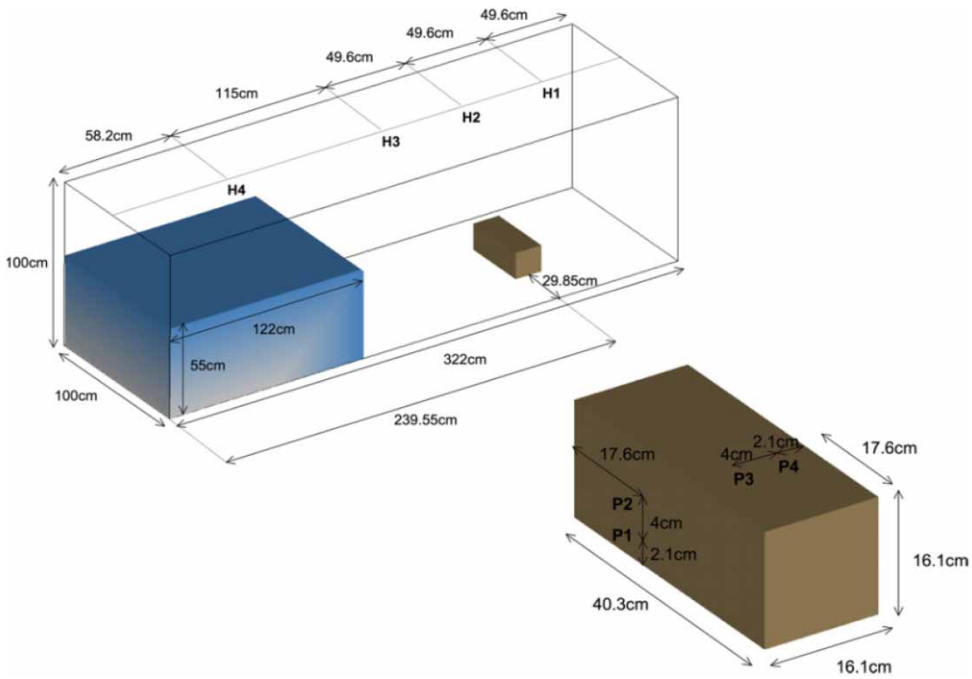

Figure 1 | Constructed physical model Case 1 (Akkerman *et al.* 2011).

obstacle was assumed. The obstacle's dimensions were 0.075 m high and 1 m base length located 1.53 m away from the plate (Figure 2).

In the third case (Soares Frazao & Testa 1999), experiments were conducted in a smooth prismatic channel of rectangular cross-section over a triangular bottom sill on the downstream bed. The column of water was 0.75 m × 15.5 m × 1.75 m. In this model the symmetrical trapezoidal-shaped bottom sill was utilized, 0.4 m high and 6 m base length, that was located 10 m downstream from the gate (Figure 3).

2.2. Numerical models and methods

In this study, ANSYS Fluent 6.3.26 was employed to conduct a series of numerical simulations on experimental model setups presented in the previous section. 3D RANS equations in Cartesian coordinate system are expressed as follows (Fluent Manual 2005):

$$\begin{cases} \dfrac{\partial \rho}{\partial t} + \dfrac{\partial}{\partial x_i}(\rho u_i) = 0 \\ \dfrac{\partial}{\partial t}(\rho u_i) + \dfrac{\partial}{\partial x_j}(\rho u_i u_j) = -\dfrac{\partial p}{\partial x_i} + \dfrac{\partial}{\partial x_j}\left[\mu\left(\dfrac{\partial u_i}{\partial x_j} + \dfrac{\partial u_j}{\partial x_i} - \dfrac{2}{3}\delta_{ij}\dfrac{\partial u_l}{\partial x_l}\right)\right] + \dfrac{\partial}{\partial x_j}(-\rho\overline{u'_i u'_j}) \end{cases} \tag{1}$$

where $i, j = 1, 2$ and 3 represent the three coordinate axes, u_1, u_2 and u_3 are the three components of velocity along x, y and z axes respectively, ρ is the density of fluid, μ is dynamic viscosity, p is pressure, t is the time and $\rho\overline{u'_i u'_j}$ is the Reynolds stresses (refer to the reference Fluent Manual 2005 for further reading). The standard k-ω model is used in the present research to solve equations of turbulent kinetic energy (k), and specific dissipation rate (ω) is based on the Wilcox k-ω model (Wilcox 1998). The k and ω equations are expressed as follows:

$$\begin{cases} \dfrac{\partial}{\partial x_i}(\rho k) + \dfrac{\partial}{\partial x_i}(\rho k u_i) = \dfrac{\partial}{\partial x_j}\left(\Gamma_k \dfrac{\partial k}{\partial x_j}\right) + G_k - Y_k + S_k \\ \dfrac{\partial}{\partial x_i}(\rho \omega) + \dfrac{\partial}{\partial x_i}(\rho \omega u_i) = \dfrac{\partial}{\partial x_j}\left(\Gamma_\omega \dfrac{\partial \omega}{\partial x_j}\right) + G_\omega - Y_\omega + S_\omega \end{cases} \tag{2}$$

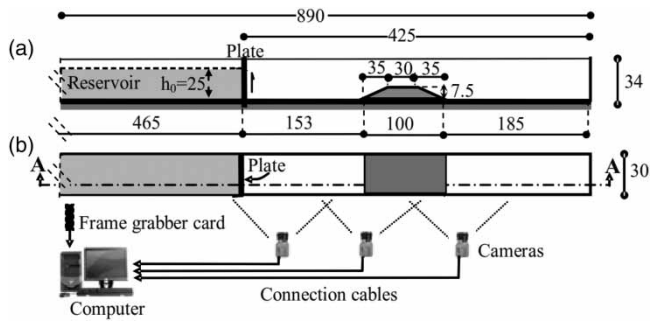

Figure 2 | Test arrangement and initial conditions of Case 2 (a) section A-A; (b) plan, lengths in cm (Ozmen-Cagatay & Kocaman 2011).

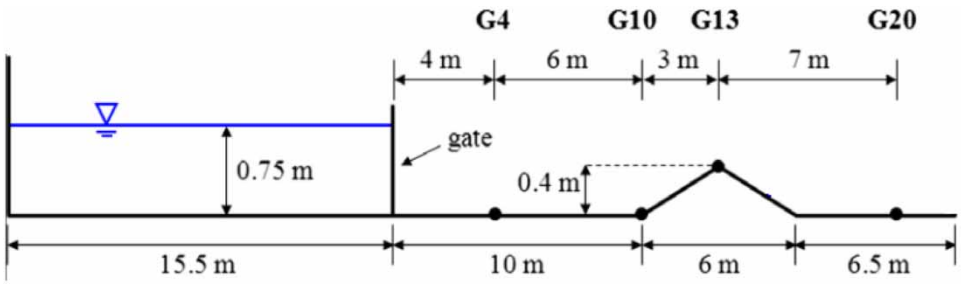

Figure 3 | Constructed physical model of Case 3 (Soares Frazao & Testa 1999).

where G_k and G_ω represent the generation of turbulence kinetic energy due to mean velocity gradients and the generation of ω respectively. Γ_k and Γ_ω represent the effective diffusivity of k and ω, respectively. Y_k and Y_ω represent the dissipation of k and ω due to turbulence. S_k and S_ω are user-defined source terms (for more information see Fluent Manual 2005).

PREssure STaggering Option (PRESTO) was applied to the pressure discretization scheme and Pressure-Implicit with Splitting of Operators (PISO) was applied to the pressure-velocity coupling (refer to reference Issa 1986). It should be noted that through a preliminary sensitivity analysis, it was found that the model with a time step equal to 0.001 seconds has negligible fluctuations and a good level of precision in the results while requiring a sufficiently short period of calculation. Hirt & Nichols (1981) proposed the VOF method for the tracking of the interface between the phases, which is accomplished by the solution of a continuity equation for the volume fraction of one (or more) of the phases. When modeling the free surface, the transport equation is solved for the qth-phase (Fluent Manual 2005),

$$\frac{\partial \alpha_q}{\partial t} + \nabla.(v.\alpha_q) = 0 \tag{3}$$

where α_q is the volume fraction of qth-phase such that where $\alpha_q = 0$ the cell is empty of the qth-phase, $\alpha_q = 1$ the cell is empty of the qth-phase, $0 < \alpha_q < 1$ the cell contains the interface between the qth-phase. In the method, by using VOF = 0.5, a free surface was defined.

2.3. Boundary conditions and mesh generation

Figure 4 illustrates the computational grid in the vicinity of the obstacles. Due to the major effects of the computational mesh on the accuracy of the obtained results, a wide range of sensitivity analyses were conducted in order to validate the suitable number of meshes. Through running the models with refined mesh sizes in various conditions, the smallest size of the mesh was approximately 1, 1.6, and 2 cm, for rectangular, trapezoidal and triangle obstacles, respectively. Figure 5 depicts the computational domains and considered channel boundaries.

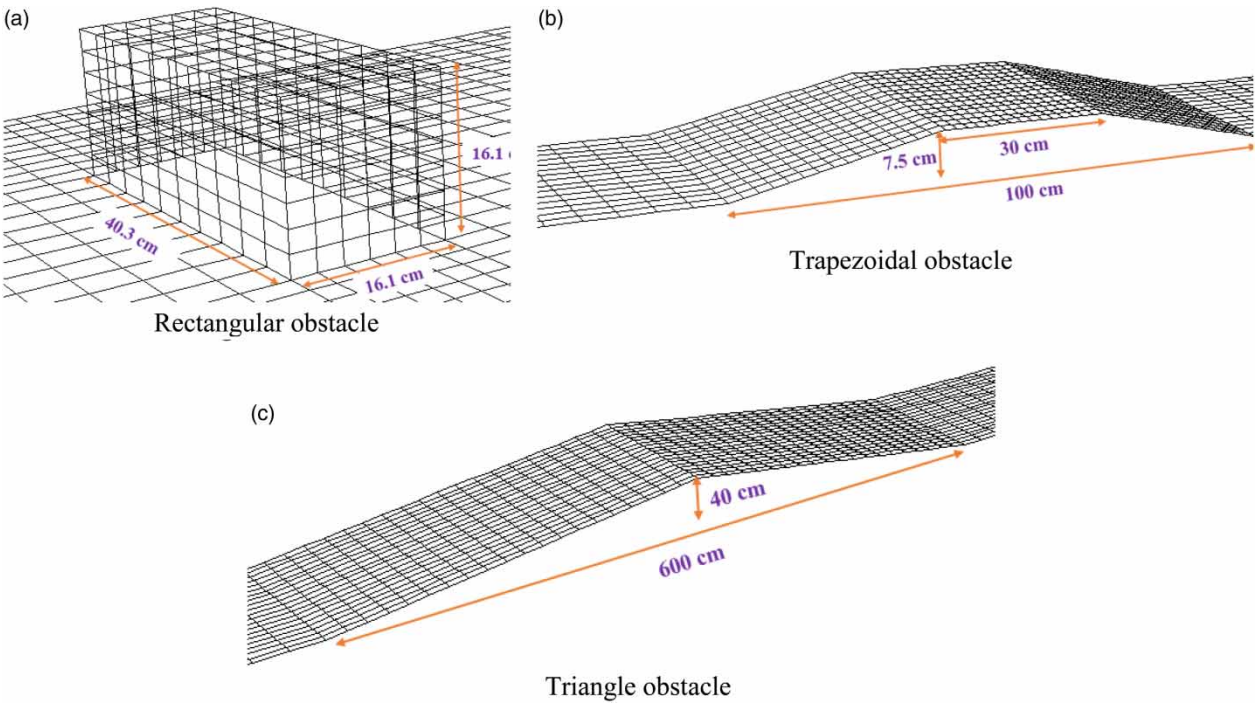

Figure 4 | Computational grid in the vicinity of the different cases.

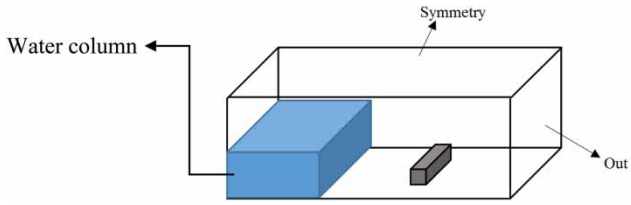

Figure 5 | Geometrical configurations and boundaries with an obstacle.

2.4. Verification of the numerical simulations

Before analyzing the results, it was necessary to ensure the accuracy of the numerical model by comparing its results with experimental measurements. For this purpose, the height of water at different points, height of free surface in the channel and pressure in different locations were investigated.

2.4.1. Dam-break flow with a rectangular obstacle

Figure 6 represents the predicted and measured time series of the water level at different gauging points H1, H2, H3 and H4 (Figure 1) for the dam-break flow with rectangle obstacle.

As can be seen from Figure 6, in point H1, it takes nearly 1 s for water to reach this point. Then the height of water at this point is increased. After about 2.5 s of breaking the dam, the water height decreases and, after 5 s, the water level rises again. Point H2, located on the obstacle, it takes about 0.43 s for water to reach this point. Then the height of water at this point is increased. Until approximately 3 s after the dam-break, the water height decreases and again, after 5 s, the water level rises. Point H3, located before the obstacle, it takes about 0.18 s for water to reach this point. Then the height of water increases at this point. Until approximately 2 s, the water height decreases, and at 2.3 s the water height reaches 0.281 m, and after 4.4 s,

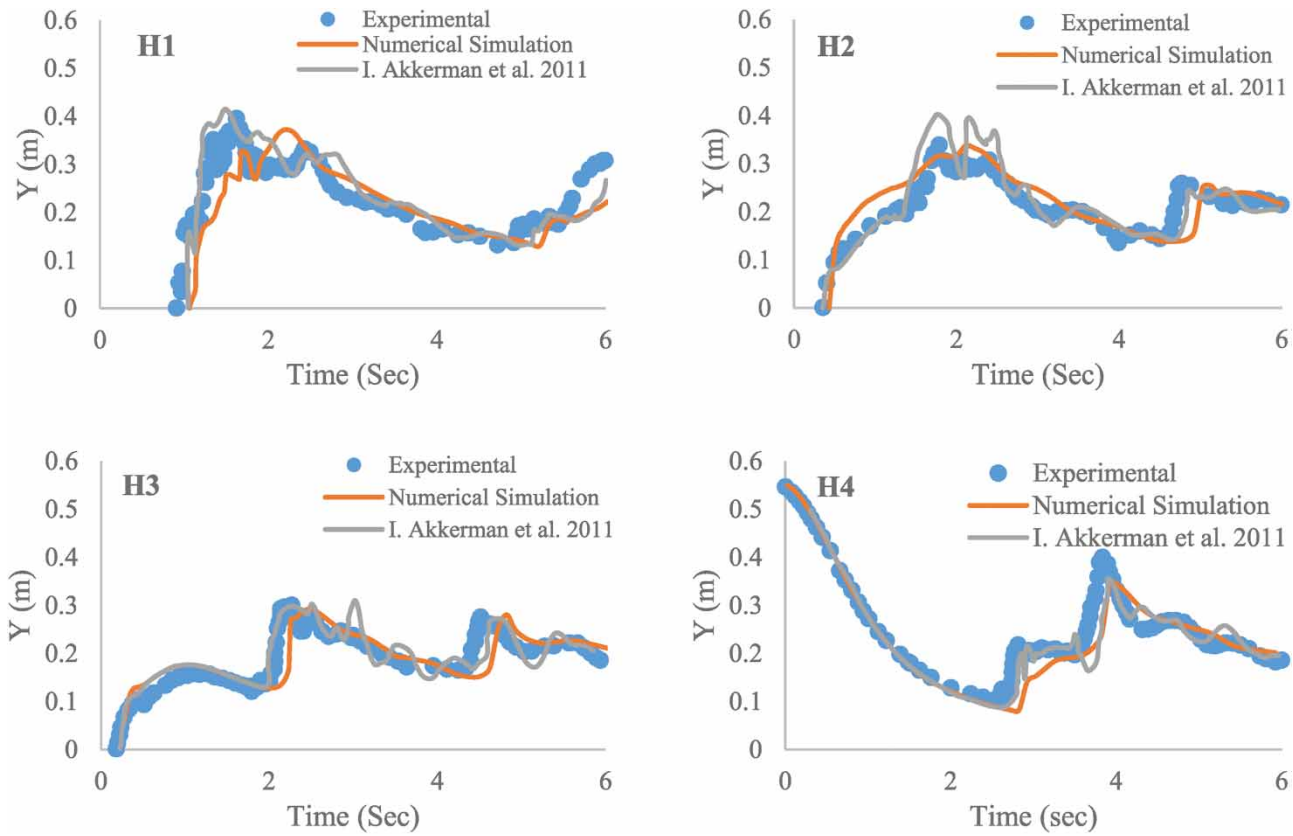

Figure 6 | Experimental and numerical results of water heights for Case 1.

the water level rises again. At point H3, all these water level fluctuations were in very good agreement with the experimental evidence. Point H4 depicts the water level fluctuations (Point H4, located on the column of water) and illustrates, first the height of water decreases, and consequently in 2.72 s the height of water falls 0.082 m. The water height decreases until 2.88 s, after that the water height reaches 0.2 m, and up to 3.62 s the water height remains stable. Then the height of water decreases again up to 3.9 s. At the time of 3.9 s the water height rises to 0.386 m and again the height of water decreases to approximately 0.2 m. In order to demonstrate the accuracy of the numerical simulations, the water pressures at different points are shown. Figure 7 represents the water pressure changes at four different locations for dam-break flow with rectangle obstacle. Figure 7 also shows the predicted and measured time histories of the water pressure at different gauging points P1 and P2 (Figure 1) for the dam-break flow with rectangle obstacle. The pressure changes over time are the same for two points. When the water reaches points 1 and 2, the pressure increases and then the pressure decreases and after a few seconds (4.82 s) the pressure rises again.

2.4.2. Dam-break flow with a trapezoidal obstacle

In this section the sudden breaking dam flow in a channel of water with a trapezoidal obstacle is considered. Figure 8 presents the predicted and measured water flow according to the four different times (based on the assumption of the model in Figure 2). Also, the effect of the trapezoidal obstacle in the case of dam-break was determined. The resulting water surface was consistent with those of laboratory results. The results indicate that after the dam-break phenomenon, a water wave moves upward in the upstream direction.

2.4.3. Dam-break flow with a triangle obstacle

In this section a comparison between the numerical modeling and the experimental data for the case of dam-break flow with a triangle obstacle is presented. Figure 9 shows the predicted and measured time-dependent water level at different gauging points G4, G10, G13 and G20 (Figure 3) for the dam-break flow with triangle obstacle.

From Figure 9, in point G4, located before the obstacle, it takes about 1.32 s for water to reach this point. Then the height of water at this point increases. Until approximately 13.16 s after the dam-break the water height increases sharply, consequently at 14.26 s, the water height is 0.512 m, and then the water height decreases. Point G10 which is located at the beginning of the obstacle, it takes about 1.32 s for water to reach this point. Then the height of water at this point increases until approximately 13.16 s after breaking the dam. The water height increases drastically, at 14.26 s the water height is 0.512 m, then the water height decreases gradually over time up to almost 40 s. In point G13, located above the obstacle, it takes about 4.27 s for water to reach this point. The water height is constant between 6.99 s and 16.42 s then the water height decreases near to zero. In point G20, located after the obstacle, the height of water is very low.

Dam-break flows with solid obstacle were successfully simulated through the comparison of the predicted results with their corresponding experimental evidence. The resulting water pressure distributions and the water surfaces at different times indicate that the standard k-ω model is an appropriate model to simulate the dam-break phenomenon with various types of obstacles.

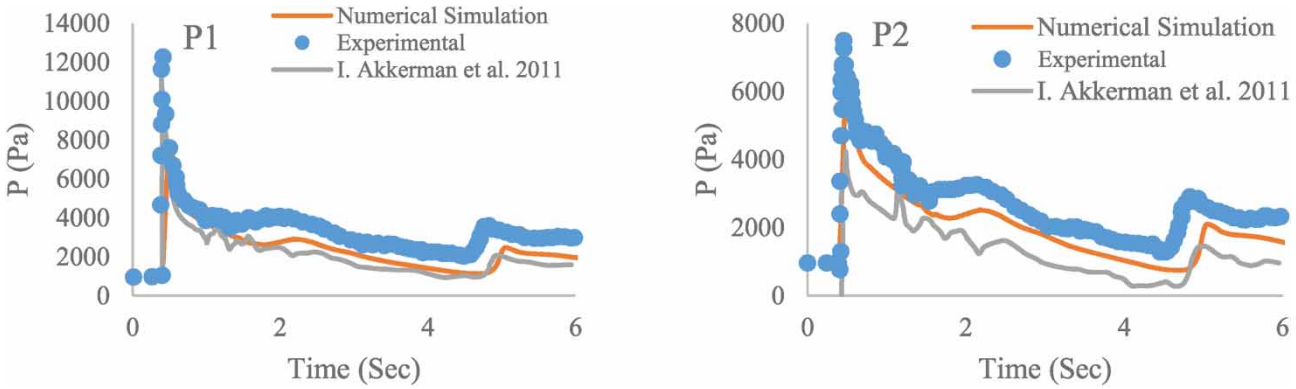

Figure 7 | Water pressures at different points for dam-break with a rectangular obstacle.

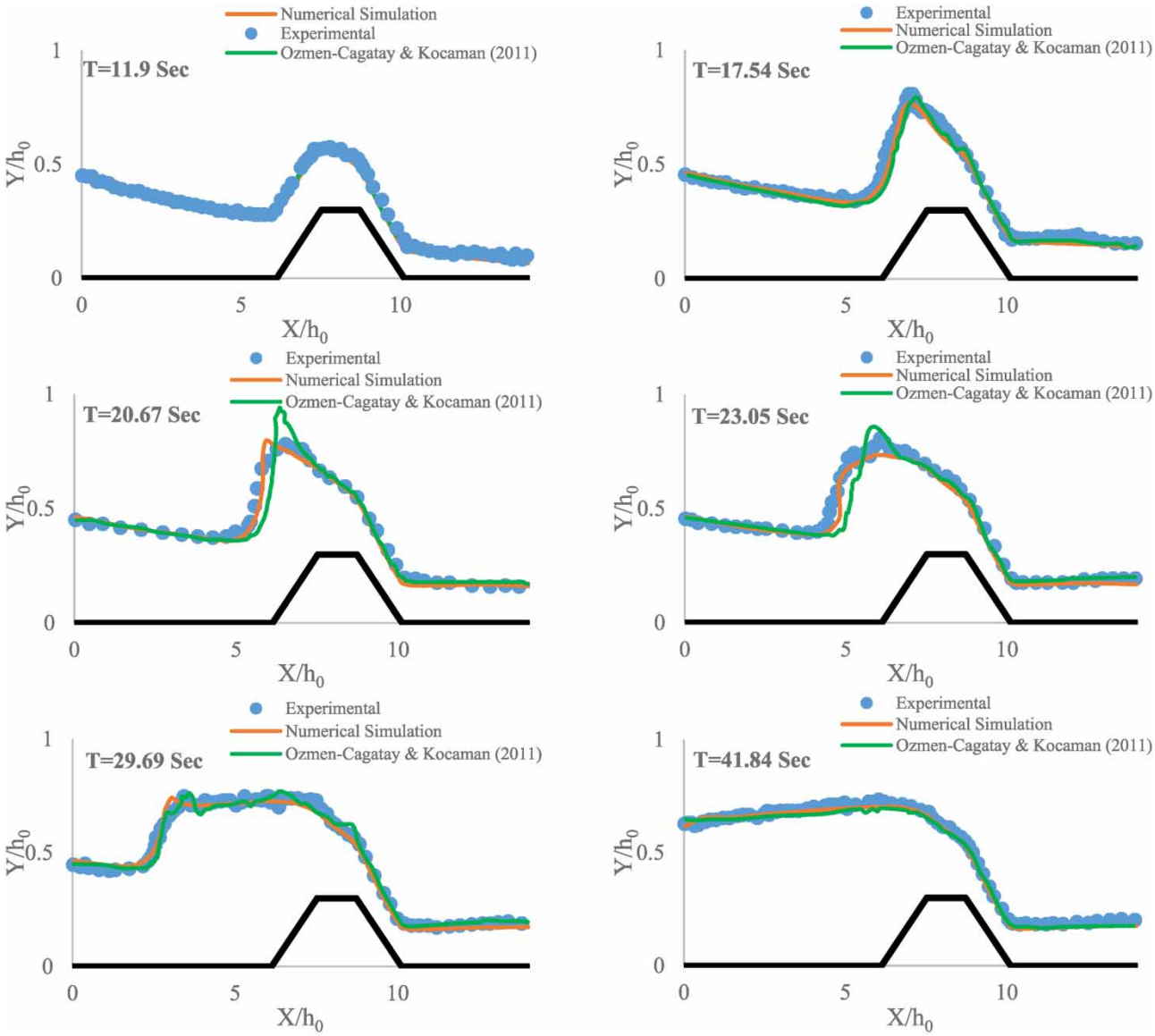

Figure 8 | Water levels at different times for the dam-break flow with trapezoidal obstacle.

3. RESULTS AND DISCUSSION

After verification, some applied results and discussions from the performed simulations are presented in this section.

3.1. 3D Free surface variations of dam-break

One of the most challenging issues during dam failure is the water level in different places, particularly in the case of an existing obstacle. For this reason, in this section the 3D water levels are investigated as follows.

Figure 10 illustrates the water profile in the case of a rectangular obstacle. Dam-break causes an unsteady flow. In less than 1 s after dam-break, the water flow faces the obstacle and immediately, the stream hits the end wall of the canal and the water bounces back. Then, after near 2 s back water flow overtops the rectangular obstacle and almost all of the obstacle is submerged. At the time of 3.5 s, the water flow hits again the beginning wall of the canal and creates a second water wave which propagates throughout the longitudinal direction of the canal. Consequently, the second wave reaches the obstacle again at the time of 4.5 s. Obviously, the second water wave has lower intensity than the first wave. However, according

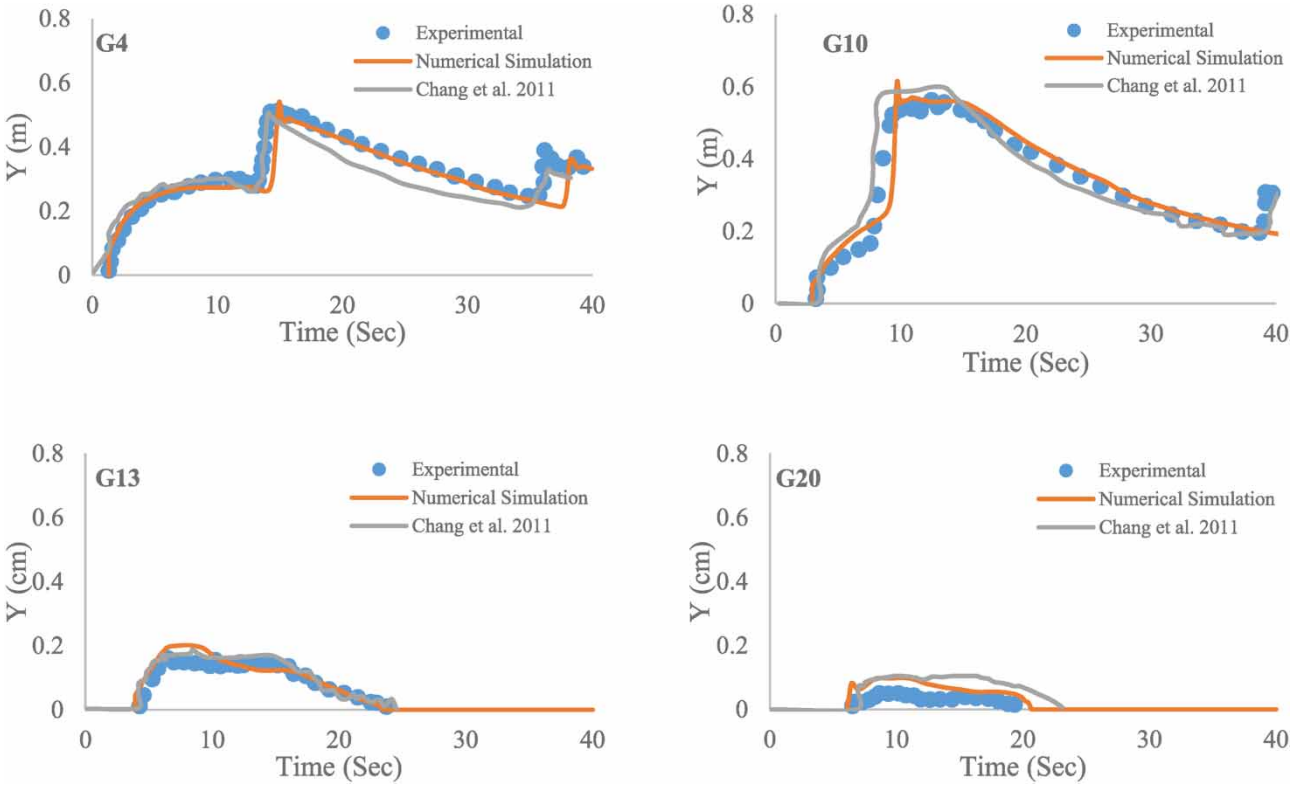

Figure 9 | Water level at different gauging points in dam-break flow with a triangle obstacle.

to Figure 10, the secondary water wave (at time 6 s) hits the end wall of the canal with lower water height. Figure 11 depicts the water surface profile at different times by considering a trapezoidal obstacle. The obstacle was located 6.18 m from the beginning wall.

In this case, in less than 1.5 s after dam breakage the water wave passes the obstacle. Moreover, at the time of 3 s due to the assumed obstacle, a wave is generated that moves upward. The wave intensity decreases when it travels to the beginning of

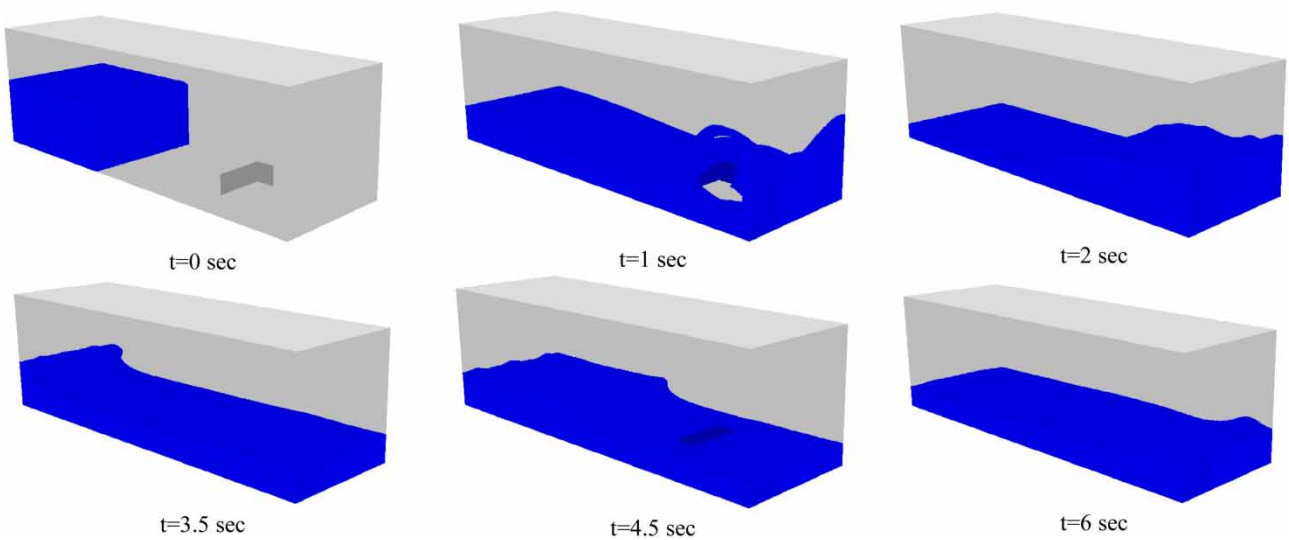

Figure 10 | 3D free surface variations of dam-break (Case 1).

the canal. Then after 11.5 s, the back water wave again hits the wall at the beginning of the canal. The generated water surface profile in the case of a triangle obstacle is shown in Figure 12.

In this case the obstacle was located at 10 m from the beginning wall. Less than 4 s after dam breakage the water wave passes the obstacle. In 7 s after breakage, the water wave reaches the end of the canal and disappears. At approximately 10 s a wave forms behind the obstacle that moves upward. After 24 s all the water in front of the obstacle totally disappeared. Figure 12 demonstrates that after 26 s from the dam breakage the back water wave reaches the beginning wall.

3.2. 3D Flow field pressure variations during break of the dam

Among all mechanical phenomena during a dam breakage, determining the pressure in different situations is much more challenging. Due to the presence of an obstacle the variation of the pressure will be in an oscillatory manner. In this regard, the variation of the pressure on the canal walls was studied (the pressures are relative to $P_o = \gamma h_o$).

According to the Figure 13, due to the reciprocating wave of water, the amount of pressure varies in different locations with respect to time. At time 1 s, the pressure reaches to $0.9\gamma h_0$ at the end of the canal. However, negative pressure reaches almost $-0.25\gamma h_0$ in the vicinity of the obstacle. The induced pressure due to the dam breakage decreases with increasing time. As a consequence, at time 3.5 s over a limited area of the canal bed the pressure is equal to $0.67\gamma h_0$. However, at 4.5 s, the area subjected to $0.67\gamma h_0$ pressure increases. Therefore, at 6 s after breakage the pressure at the canal bed decreases near to $0.67\gamma h_0$ and at the same time other bed surfaces experience pressure lower than $0.67\gamma h_0$.

In Figure 14, unlike the rectangular obstacle, due to the drainage of water flow from the downstream and also because of the rather long distance between the dam axis and the obstacle, the induced pressure decreases over time. Hence, at 1.5 s the pressure at the bed of the canal reaches near to γh_0 and at the moment lower pressure occurs at the obstacle. After water wave completion impact at about 3 s after breakage, the induced pressure reaches near to $0.6\gamma h_0$ in the vicinity of the obstacle. As

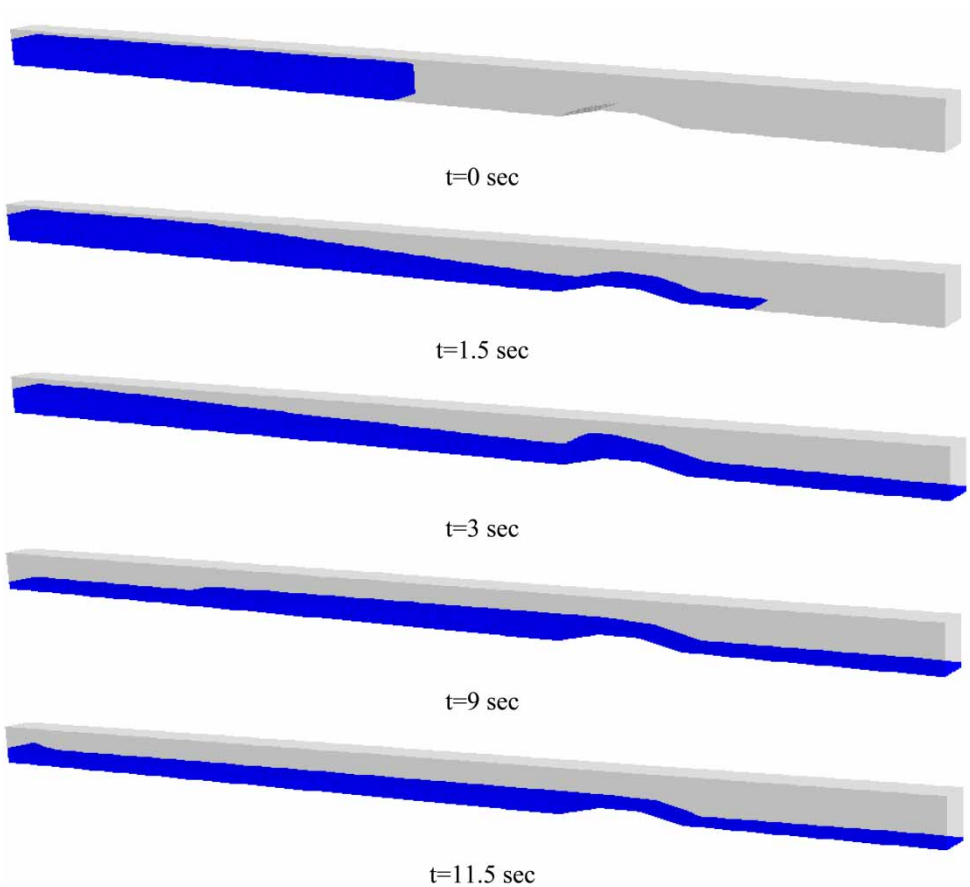

Figure 11 | 3D free surface variations of dam-break (Case 2).

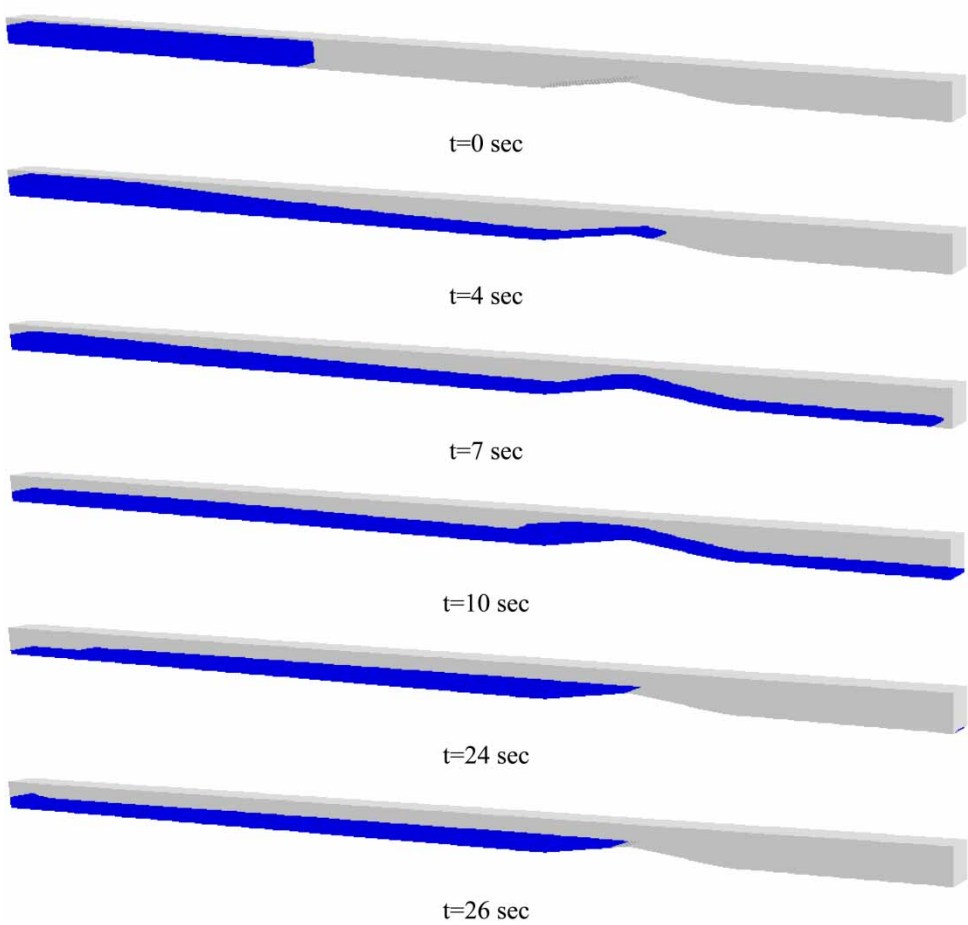

Figure 12 | 3D free surface variations of dam-break (Case 3).

time progresses and associated with the returning of the wave water to the upstream, the pressure at the bed of the canal increases; however, the pressure decreases with increasing time.

In Figure 15, similar to the trapezoidal obstacle, in the case of a triangle obstacle with disappearing water from the downstream side, the pressure at different times decreased. Hence, at 4 s, the pressure at the bed of the canal reaches near to γh_0 and at this time lower pressure occurs at the obstacle. After water wave completion impact at about 10 s after breakage, the induced pressure reaches near to $0.8\gamma h_0$ in the vicinity of the obstacle. After a time and by returning the wave water to the upstream, the pressure at the bed of the canal increases; however, the pressure decreases with increasing time.

3.3. 3D Flow field velocity variations during break of the dam

When there is a dam-break, by considering the water depths and presence of the obstacle, variation of the water flow velocities, particularly around the obstacle is of significant importance.

Figure 16 depicts the water velocities throughout a canal with a rectangular obstacle. At the time of 1 s, the velocity equal to 3 m/s is observed. At time 2 s and after the water wave hits the downstream wall, the velocity decreases near to 1.2 m/s. At 3.5 s, when the water wave reaches the initial wall, a uniform distribution of velocities occurred. However, at 4.5 s due to the wave traveling in the downstream direction, the velocity of the upper layer of the water wave reaches again 1.8 m/s. Consequently, by decreasing the water wave energy, some time after the dam-break the velocities decreased.

Figure 17 illustrates the water velocities throughout a canal with a trapezoidal obstacle. Due to the presence of an obstacle, the nature of the velocity distribution in time is oscillatory. After 1.5 s of dam-break the velocity is 2 m/s. At time 3 s, the situation of the maximum velocity moves forward along the downstream. Consequently, by completion of the reflected water

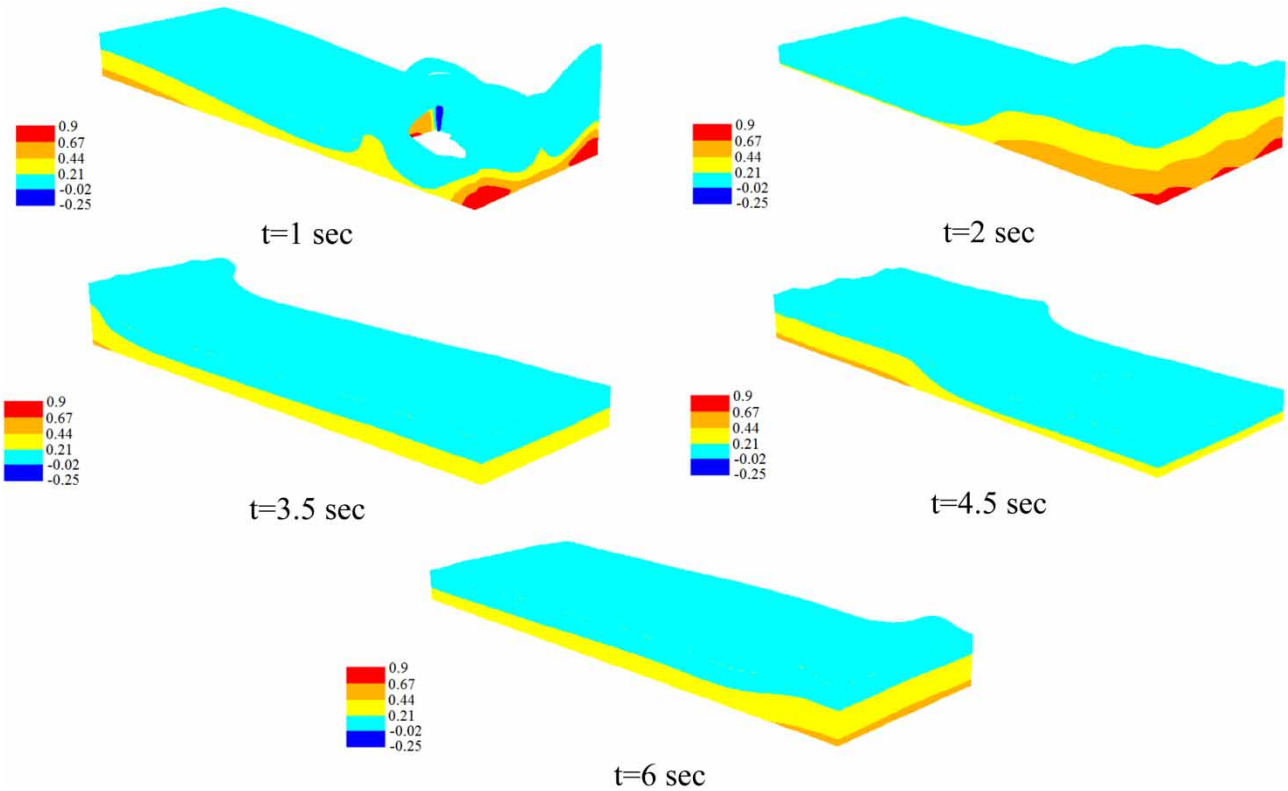

Figure 13 | Flow field pressure variations during dam breakage (Case 1).

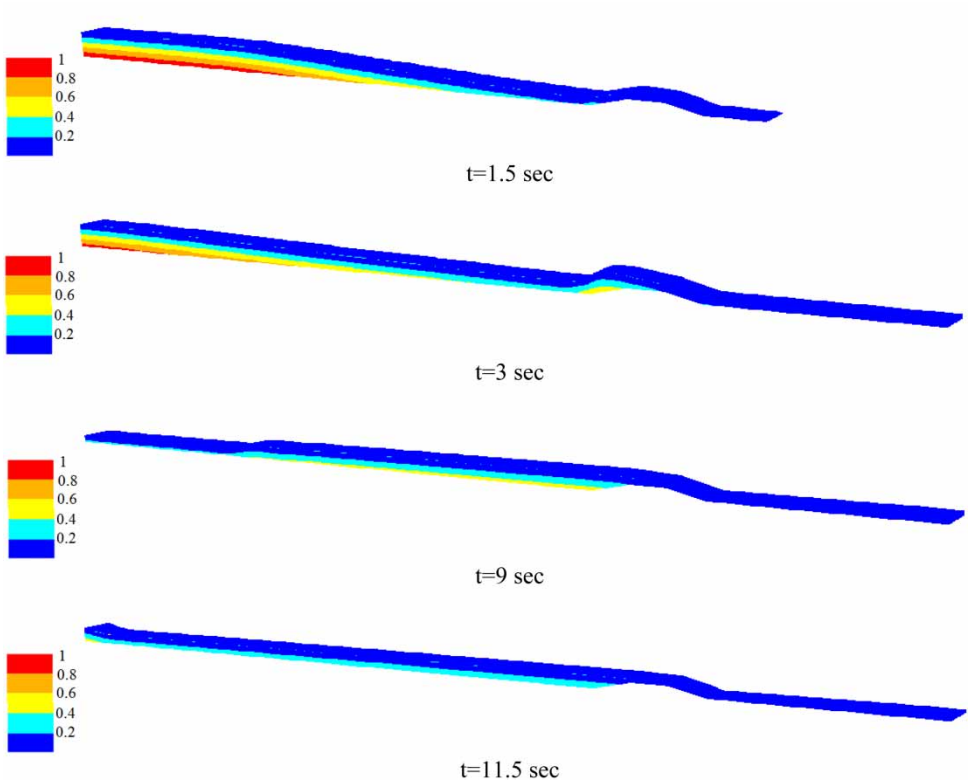

Figure 14 | Flow field pressure variations during dam breakage (Case 2).

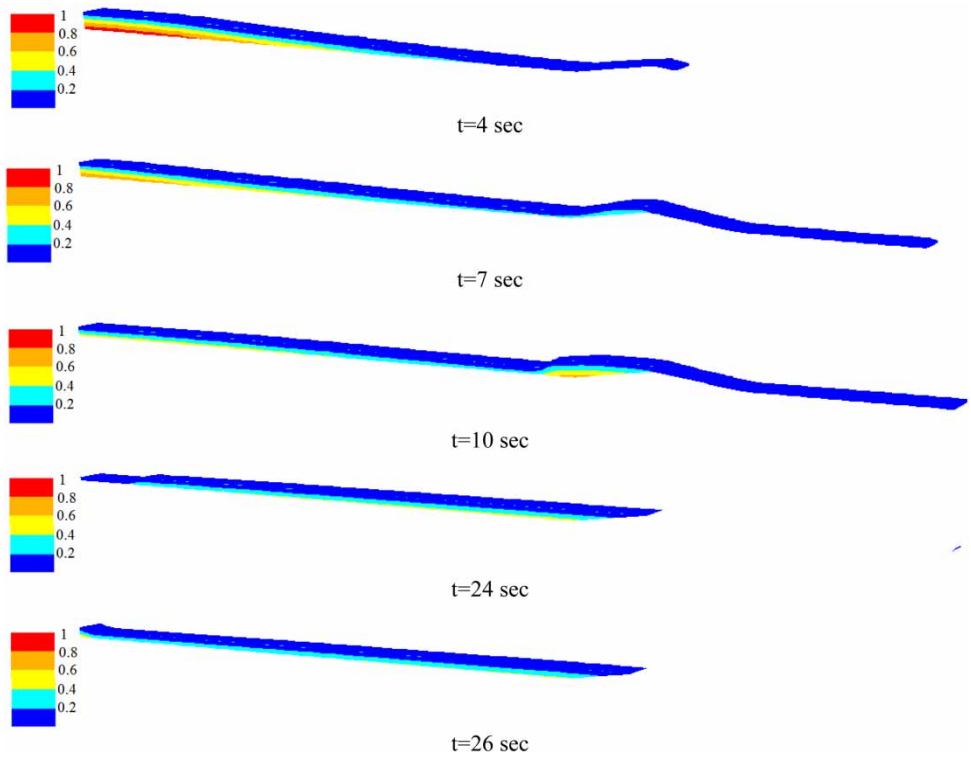

Figure 15 | Flow field pressure variations during dam breakage (Case 3).

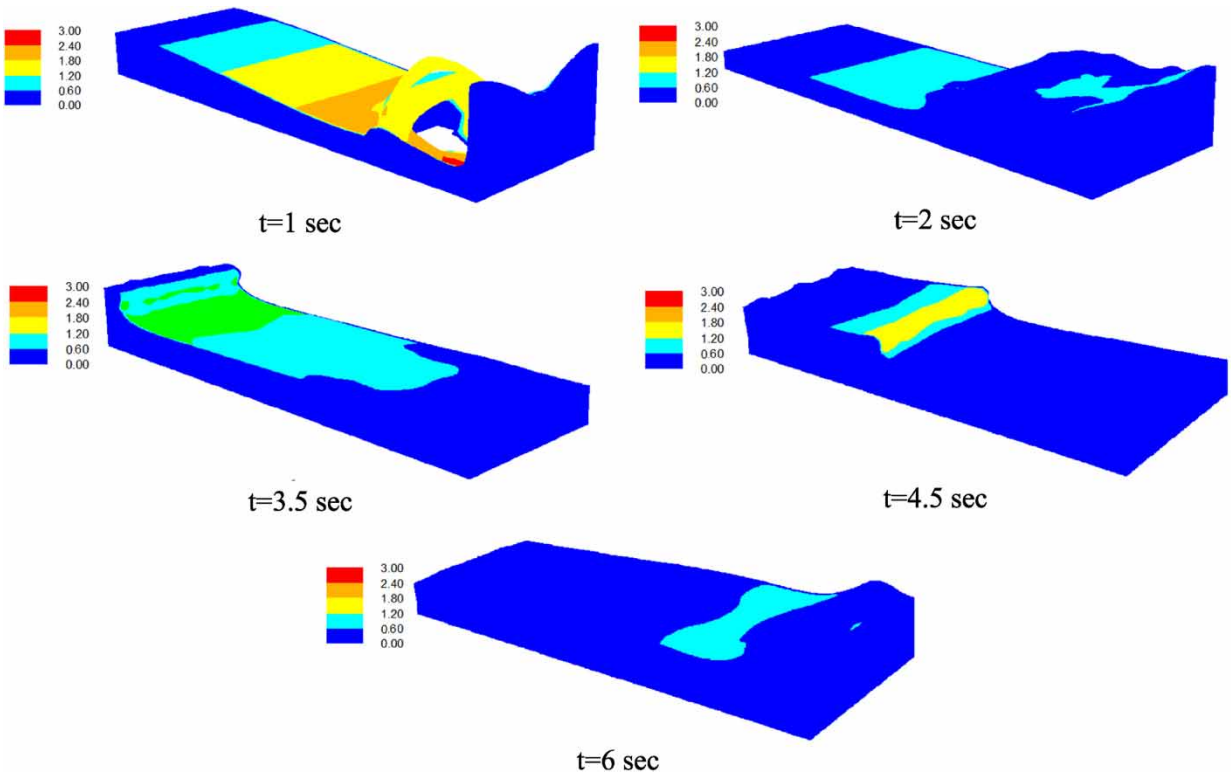

Figure 16 | Flow field velocity variations during break of the dam (Case 1).

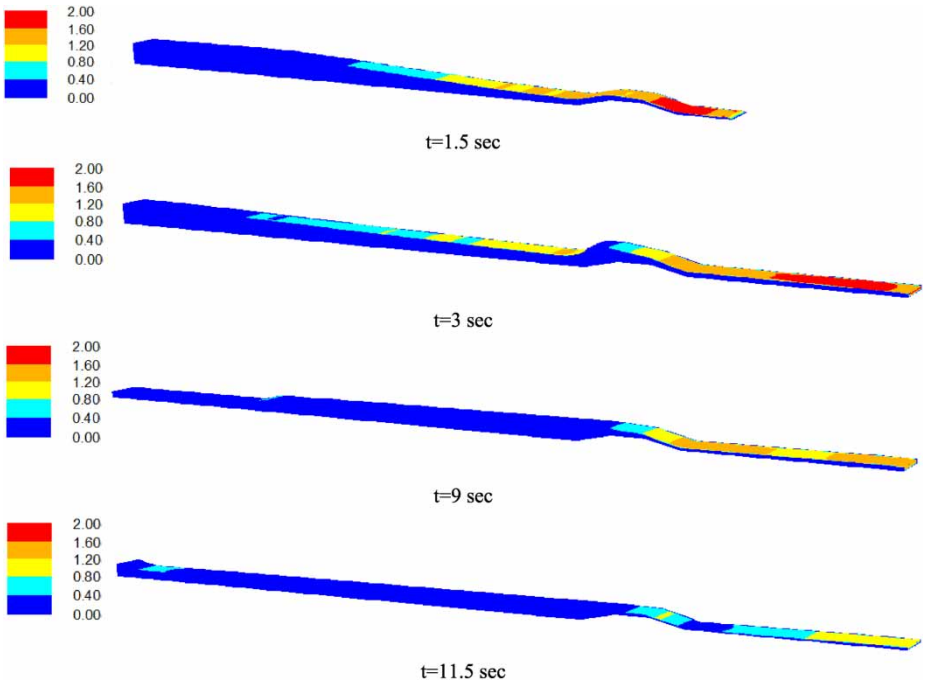

Figure 17 | Flow field velocity variations during break of the dam (Case 2).

wave, maximum downstream velocity decreased to a value near to 1.6 m/s. At this moment, the maximum upstream velocity also decreased to 0.4 m/s with some local velocities near to 0.8 m/s.

Like the trapezoidal obstacle, when a triangle obstacle is considered against water flow, an oscillatory flow results. Figure 18 shows the variation of velocity over time for a triangle obstacle. At 4 s, the velocity approaches 3.25 m/s around the obstacle.

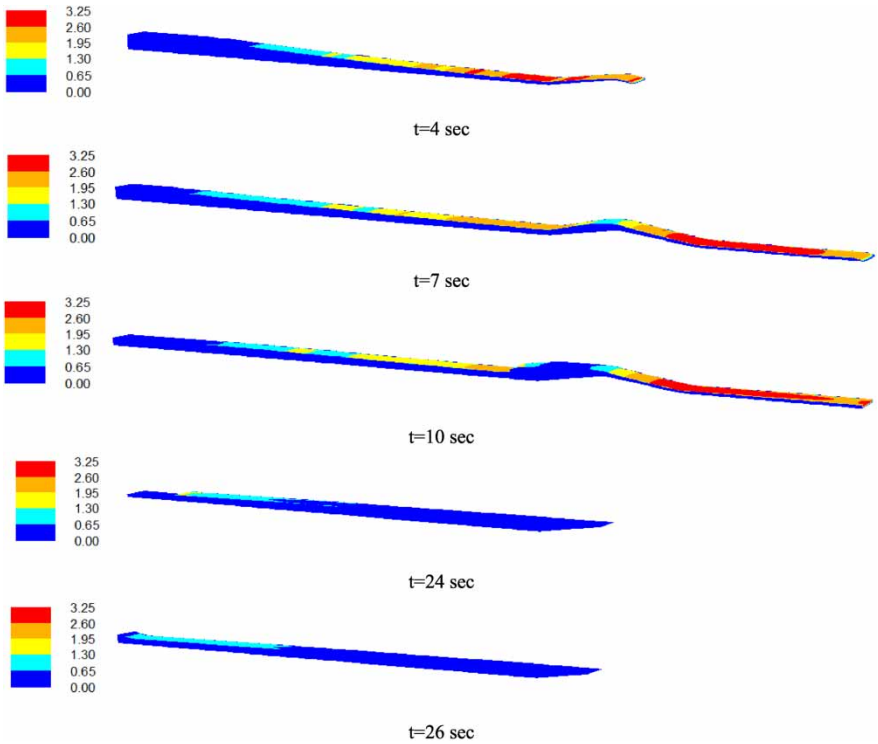

Figure 18 | Flow field velocity variations during break of the dam (Case 3).

After the obstacle and due to the similar bed slope, the velocity remains at about 3.25 m/s until 10 s from the dam-break. However, after about 24 s, the downstream flow completely disappeared and only upstream back flow in front of the obstacle continues with 1.3 m/s velocity.

4. SUMMARY AND CONCLUSIONS

In this paper, a 3D model of dam-break flow over different obstacles with dry beds was developed. To verify the Fluent software performance, the height of water at different points, the height of free surface in the channel and pressure in different locations with rectangular, triangular and trapezoidal obstacles were investigated. Simulations were performed with the standard k-ω turbulent model, the PISO pressure-velocity coupling scheme and the VOF method for tracking the free surface. By comparing the 3D-simulation results with dam-break flows over the different obstacles, it was found that the numerical models have sufficient accuracy and were in agreement with experimental data and results of other researches. Furthermore, the results showed that if there was a wall at the end of the channel and the distance between the barriers at the end wall was small (Case 1), maximum water height occurred after the flow collided with the end wall. If the end of the channel was open (Cases 2 and 3), the maximum water height occurred after the current hit the obstacle. In the rectangular obstacle, negative pressure happened in the vicinity of the obstacle, while in the trapezoidal and triangular obstacles, the pressure was always positive. The maximum velocity happened at the front of the wave causing dam-break. Over time and by the return of the water wave, the velocity decreased dramatically.

DATA AVAILABILITY STATEMENT

All relevant data are included in the paper or its Supplementary Information.

REFERENCES

Akkerman, I., Bazilevs, Y. E., Kees, C. & Farthing, M. W. 2011 Isogeometric analysis of free-surface flow. *Journal of Computational Physics* **230** (11), 4137–4152.

Amini, R., Maghsoodi, R. & Moghaddam, N. 2016 Simulating free surface problem using isogeometric analysis. *Journal of the Brazilian Society of Mechanical Sciences and Engineering* **38** (2), 413–421.

Celis, M., Wanderley, J. & Neves, M. 2017 Numerical simulation of dam breaking and the influence of sloshing on the transfer of water between compartments. *Ocean Engineering* **146**, 125–139.

Chang, T. J., Kao, H. M., Chang, K. H. & Hsu, M. H. 2011 Numerical simulation of shallow-water dam break flows in open channels using smoothed particle hydrodynamics. *Journal of Hydrology* **408** (1–2), 78–90.

Dressler, R. F. 1952 *Hydraulic Resistance Effect upon the Dam-Break Functions*. National Bureau of Standards, Washington, DC.

Fluent Manual 2005 *Manual and User Guide of Fluent Software*. Fluent Inc., New York.

Goater, A. J. & Hogg, A. J. 2011 Bounded dam-break flows with tailwaters. *Journal of Fluid Mechanics* **686**, 160–186.

Gu, Z. H., Wen, H. L., Yu, C. H. & Sheu, T. W. H. 2018 Interface-preserving level set method for simulating dam-break flows. *Journal of Computational Physics* **374**, 249–280.

Heo, Z., Wu, T., Weng, H., Hu, P. & Wu, G. 2017 Numerical simulation of dam-break flow and bed change considering the vegetation effects. *International Journal of Sediment Research* **32** (1), 105–120.

Hirt, C. W. & Nichols, B. D. 1981 Volume of fluid (VOF) method for the dynamics of free boundaries. *Journal of Computational Physics* **39** (1), 201–225.

Issa, R. I. 1986 Solution of the implicitly discretised fluid flow equations by operator-splitting. *Journal of Computational Physics* **62** (1), 40–65.

Issakhov, A., Zhandaulet, Y. & Nogaeva, A. 2018 Numerical simulation of dam break flow for various forms of the obstacle by VOF method. *International Journal of Multiphase Flow* **109**, 191–206.

Lauber, G. & Hager, W. H. 1998 Experiments to dambreak wave: horizontal channel. *Journal of Hydraulic Research* **36** (3), 291–307.

Lobovský, L., Botia-Vera, E., Castellana, F., Mas-Soler, J. & Souto-Iglesias, A. 2014 Experimental investigation of dynamic pressure loads during dam break. *Journal of Fluids and Structures* **48**, 407–434.

Maghsoodi, R., Roozgar, M. S., Chau, K. W. & Sarkardeh, H. 2012 3D simulation of dam break flows. *Dam Engineering* **23** (2), 53–70.

Morris, M. 2000 *Concerted Action on Dam Break Modeling Final Report–CADAM*, HR Wallingford, Wallingford, UK.

Munoz, D. H. & Constantinescu, G. 2020 3-D dam break flow simulations in simplified and complex domains. *Advances in Water Resources* **137**, 103510.

Ozmen-Cagatay, H. & Kocaman, S. 2011 Dam-break flow in the presence of obstacle: experiment and CFD simulation. *Engineering Applications of Computational Fluid Mechanics* **5** (4), 541–552.

Ritter, A. 1892 Die fortpflanzung de wasserwellen. *Zeitschrift Verein Deutscher Ingenieure* **36** (33), 947–954.

Seyedashraf, O., Rezaei, A. & Akhtari, A. A. 2017 Dam break flow solution using artificial neural network. *Ocean Engineering* **142**, 125–132.

Shobeyri, G. & Afshar, M. 2010 Simulating free surface problems using discrete least squares meshless method. *Computers & Fluids* **39** (3), 461–470.

Soares Frazao, S. & Testa, G. 1999 The Toce River test case: numerical results analysis. In: *Proceedings of the 3rd CADAM Workshop*, Milan, Italy.

Soares-Frazão, S. & Zech, Y. 2007 Experimental study of dam-break flow against an isolated obstacle. *Journal of Hydraulic Research* **45** (sup1), 27–36.

Vosoughi, F., Rakhshndehroo, G., Nikoo, M. R. & Sadegh, M. 2020 Experimental study and numerical verification of silted-up dam break. *Journal of Hydrology* **590**, 125267.

Wang, L.-h. & Pan, C.-h. 2015 An analysis of dam-break flow on slope. *Journal of Hydrodynamics, Series B* **26** (6), 902–911.

Wilcox, D. C. 1998 *Turbulence Modeling for CFD*, Vol. 2. DCW Industries Inc., La Canada, CA.

Yang, S., Yang, W., Qin, S., Li, Q. & Yang, B. 2018 Numerical study on characteristics of dam-break wave. *Ocean Engineering* **159**, 358–371.

Ye, Y., Xu, T. & Zhu, D. Z. 2020 Numerical analysis of dam-break waves propagating over dry and wet beds by the mesh-free method. *Ocean Engineering* **217**, 107969.

Yu, Z., Feng, N. & Glotko, A. 2016 The forecast of flooding resulting from dam break near Nizhny Novgorod. *Procedia Engineering* **154**, 1306–1313.

First received 19 October 2021; accepted in revised form 10 January 2022. Available online 28 January 2022